Vol 11 No 8, August 2002
1009-1963/2002/11(08)/0827-07

Chinese Physics

© 2002 Chin. Phys. Soc.
and IOP Publishing Ltd

Zero-field-cooled and field-cooled magnetizations and magnetic susceptibility of itinerant ferromagnet $SrRuO_3$ *

Hou Deng-Lu(侯登录)[a)b)], Jiang En-Yong(姜恩永)[a)], and Bai Hai-Li(白海力)[a)]

[a)] *Department of Applied Physics, Tianjin University, Tianjin 300072, China*

[b)] *Department of Physics, Hebei Normal University, Shijiazhuang 050016, China*

(Received 14 December 2001; revised manuscript received 25 March 2002)

Zero-field-cooled (ZFC) magnetization, field-cooled (FC) magnetization, ac magnetic susceptibility and major hysteresis loops of itinerant ferromagnet $SrRuO_3$ have been measured at magnetic ordering temperatures ranging from 5 to 160 K. An empirical model is proposed to calculate the measured ZFC magnetization. The result indicates that the calculated ZFC magnetization compares well with the measured one. Based on the generalized Preisach model, both the ZFC and FC curves are reproduced by numerical simulations. The critical temperature and critical exponents are determined by measuring the ac magnetic susceptibility in different bias magnetic fields at temperatures in the vicinity of the point of phase transition.

Keywords: zero-field-cooled magnetization, field-cooled magnetization, magnetic susceptibility, hysteresis loop

PACC: 7560E, 7540C, 7530C

1. Introduction

From the point of view of potential technological applications, the similarity of crystal structure and lattice constants existing between $SrRuO_3$ and YBCO high-T_C superconducting oxides makes $SrRuO_3$ a promising candidate for the fabrication of Josephson junctions. In addition, the 'bad-metal' conducting characteristic of $SrRuO_3$ makes it a suitable material for the electrodes of devices based on perovskite oxides. The actual nature of the magnetism of $SrRuO_3$, usually considered as pure itinerant magnetism, has not been fully understood yet.[1−4] The Curie temperature of $SrRuO_3$ falls in a wide range of 120–167K. The measured saturation magnetic moment of Ru in $SrRuO_3$ is 1.1 μ_B, which is much smaller than the calculated value of 2 μ_B for a low-spin Ru^{4+} state, while its effective magnetic moment of 2.60 μ_B, measured in the paramagnetic region, is quite close to the expected value of 2.83 μ_B for Ru^{4+}.[3] Interestingly, a highly correlated metal $CaRuO_3$, which has the same crystal structure and similar effective Ru moment as $SrRuO_3$, remains paramagnetic at very low temperature even down to 1K.[5]

Experimentally, $SrRuO_3$ presents very interesting zero-field-cooled (ZFC) and field-cooled (FC) magnetization curves. Many explanations to these behaviours have been suggested in the literature. Joy *et al*[6] calculated the ZFC curve of $SrRuO_3$ by using a notation of 'susceptibility'. Compared with experimental curves, although the similar shape of ZFC curves were obtained, a large discrepancy exists in the magnitude of magnetization for highly anisotropic compounds such as $SrRuO_3$. Kumar *et al*[7] analysed the ZFC behaviours of $La_{0.5}Sr_{0.5}CoO_3$ and $SrRuO_3$ in low magnetic field, and concluded that the cluster-glass-like behaviour of $La_{0.5}Sr_{0.5}CoO_3$ originates from its magnetocrystalline anisotropy. It has also been reported[8] that there is a direct correlation between the shapes of ZFC curves and the domain structure.

In this paper, we focus on the ZFC and FC magnetization curves of $SrRuO_3$ recorded in a sequence of applied fields, as well as its susceptibility measured at different bias magnetic fields.

2. Experimental details

Polycrystalline $SrRuO_3$ samples were synthesized by a conventional solid-state chemical reaction.[2]

*Project supported by the National Natural Science Foundation of China (Grant Nos 50072015, 50172033).

†Author to whom any correspondence should be addressed. Tel:+86-22-27406991, Fax: +86-22-27403425, email: houdenglu@eyou.com

Room temperature x-ray diffraction indicates a pure orthorhombic distorted perovskite structure with a=0.5548±0.0002 nm, b=0.5551±0.0005 nm and c=0.7830±0.0004 nm. Scanning electron microscopy (SEM) analyses reveal that the mean diameter of the crystalline particles is about 1.5 μm. Measurements of the ac susceptibility (at 2.4kHz in 0.1Oe rms driving field) and dc magnetization were carried out in a Quantum Design Model PPMS 6000 magnetometer on a 27.6 mg polycrystalline sample of approximate dimensions 1.0 × 1.0 × 6.2 mm^3. The major hysteresis loops were measured with the maximum field of 40 kOe. ZFC magnetization and FC magnetization were measured as stated in Ref.[9].

3. Results and discussion

3.1. Analysis of ZFC magnetization using an empirical model

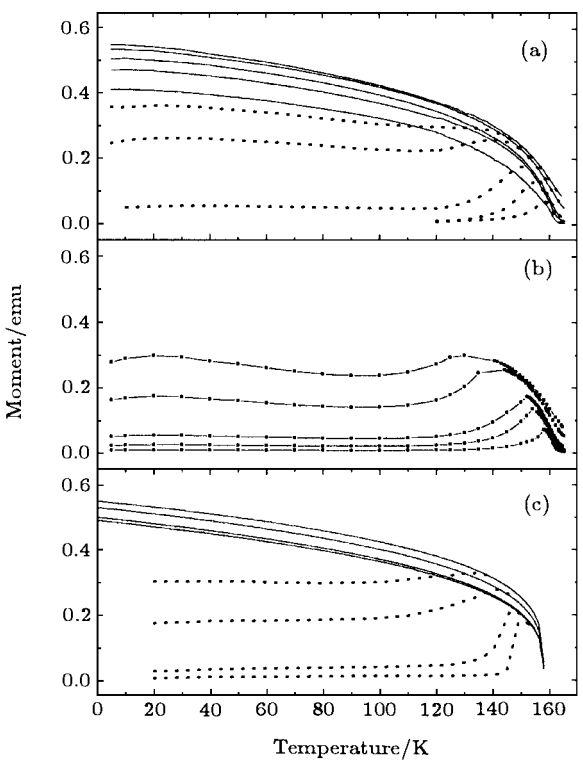


Fig.1. The FC (solid curves) and ZFC (dotted curves) magnetizations as functions of temperature measured at applied fields H_A=200, 500, 1000, 3000 and 5000 Oe, bottom to top. (b) The calculated ZFC magnetization using an empirical model: H_A=200, 500, 1000, 3000 and 5000 Oe, bottom to top. (c) Numerical simulations of the FC (solid curves) and ZFC (dotted curves) data by the Preisach model: H_A=500, 1000, 3000 and 5000 Oe, bottom to top.

Fig.1(a) shows the FC and ZFC magnetizations as a function of temperature at applied fields H_A=200, 500, 1000, 3000 and 5000 Oe. From the figure, the following features are noticeable. (1) All $M_{\rm FC}$ curves are similar, and decrease monotonically with temperature. (2) Each $M_{\rm ZFC}$ curve shows a peak at a certain temperature T_P. (3) The $M_{\rm ZFC}$ peak shifts to low temperature as the applied field increases. (4) At temperatures higher than the peak temperature T_P, the $M_{\rm ZFC}$ and $M_{\rm FC}$ curves merge together.

In order to explain the temperature dependence of ZFC magnetization, $M_{\rm ZFC}(T)$, it is necessary to review the magnetic moment behaviours in ZFC and FC processes. When the sample is cooled in a non-zero field (FC), the spin moments are ordered, and almost parallel to the direction of applied field. Thus non-zero magnetization is visible even if the field decreases down to zero. In this case, the $M_{\rm FC}(T)$ behaviour is similar to the behaviour of spontaneous magnetization, and can easily be explained.

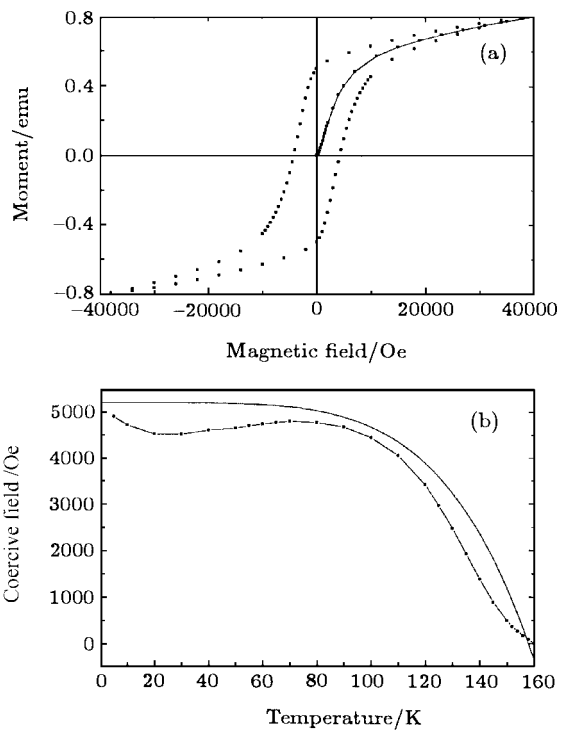


Fig.2. (a) The major hysteresis loop and initial magnetization curve at 5 K. (b) A comparison of the measured coercivity $H_{\rm C}$ (discrete points) and the model coercivity $\overline{h}_c$ (curve) from the Preisach numerical simulations.

When the sample experiences a ZFC process, its spin moments are totally disordered, showing zero magnetization when the field is zero. If a field H_A is applied to the sample at low temperatures, some spin moments rotate to the external field direction,

and the sample shows net magnetization. Usually, a large applied field (H_A) and a large spontaneous magnetization (or $M_{\rm FC}$) produce a large ZFC magnetization. But the magnetic anisotropy resists the moment rotation to the applied field direction. From the initial magnetization curve (Fig.2(a)), it is obvious that when the applied field is as large as the coercivity, $M_{\rm ZFC}$ is about half of $M_{\rm FC}$. For simplification, assuming $M_{\rm ZFC}$ is proportional to applied field H_A and $M_{\rm FC}$, but inversely proportional to magnetic anisotropy or coercivity $H_{\rm C}$, we have

$$M_{\rm ZFC}(T) = M_{\rm FC}(T) \times \frac{H_A}{2H_{\rm C}}, (H_A < 2H_{\rm C}). \qquad (1)$$

It is clear that this equation is reasonable when the calculated $M_{\rm ZFC}$ is smaller than the $M_{\rm FC}$, i.e. $H_A < 2H_{\rm C}$. For the region of $H_A \geq 2H_{\rm C}$, we let $M_{\rm ZFC} = M_{\rm FC}$.

Equation (1) shows the relationship between ZFC and FC magnetizations by virtue of coercivity, and it can be used to explain the shape and magnitude of the measured ZFC curves. It predicts that the shape of the ZFC curve (showing a peak or not) originates from the temperature dependence of coercivity. Fortunately, different ZFC behaviours have been observed in various materials,[8,10,11] and they can all be explained by virtue of this empirical model.

Measuring the major hysteresis loops at temperatures ranging from 5 to 160 K, we obtained the coercivity versus temperature curve, as shown in Fig.2(b). $M_{\rm ZFC}$ can thus be calculated by applying Eq.(1). The measured and calculated $M_{\rm ZFC}$ are similar both in shape and magnitude (see Figs.1(a) and (b)). Considering the simplicity of the empirical assumptions, we can say that they are roughly in agreement. Using the empirical model, some explanations to the $M_{\rm ZFC}$ curves of $SrRuO_3$ can be given. (1) According to Eq.(1), if the coercivity decreases faster than $M_{\rm FC}(T)$ with increasing temperature, $M_{\rm ZFC}(T)$ increases. When $M_{\rm ZFC}$ reaches the value of $M_{\rm FC}$ at a certain temperature, $M_{\rm ZFC}$ and $M_{\rm FC}$ decrease together with a further increase of temperature. Obviously the peak in the ZFC curve originates from the different temperature dependence of FC magnetization and coercivity. (2) The $M_{\rm ZFC}(T)$ peak appears when the coercivity $H_{\rm C}(T)$ equals $H_A/2$. For a higher applied field H_A, the $M_{\rm ZFC}(T)$ peak will appear at a lower temperature where $H_{\rm C}(T) = H_A/2$ is larger; while for a lower applied field H_A, the $M_{\rm ZFC}(T)$ peak will appear at a higher temperature where $H_{\rm C}(T) = H_A/2$ is smaller. This can be employed to explain why the ZFC peaks shift to lower temperature with the applied field increasing. (3) When the applied field is lower, the difference between ZFC and FC magnetizations is larger at lower temperatures. According to Eq.(1), this is because the coercivity is much larger than the applied field at lower temperatures. This point of view is different from that of 'spin glass behaviours' discussed in the literature.[2]

In fact, the dependence of $M_{\rm ZFC}$ on applied field H_A at a certain temperature, i.e. $M_{\rm ZFC}(H_A)|_{T=T_0}$, is the initial magnetization curve at this temperature (see Fig.2(a)). So it is inevitable that some differences exist between calculated and measured $M_{\rm ZFC}$, especially when the applied field is equal to, or larger than, the coercivity. Therefore, it is necessary to further discuss the behaviours of ZFC and FC magnetizations.

3.2. Analysis of ZFC and FC magnetizations by the Preisach model

The strength of the Preisach model on hysteresis[12] ultimately resides in its unique combination of physical generality and mathematical simplicity. The model has been described in some detail in the literature,[9] and only a brief summary is provided here. All magnetic systems are represented by a collection of Barkhausen instabilities, each with moment μ, two energy barriers $W_{\pm}$, a dissipative (coercive) field $h_c = (W_+ + W_-)/2\mu$, and an asymmetric (interaction) field $h_i = (W_+ - W_-)/2\mu$. The Barkhausen spectrum is described by a temperature-dependent distribution $P(\mu, h_c, h_i, T)$. For the particular system investigated here

$$P(\mu, h_c, h_i, T) = \delta(\mu - \mu_0(T)) \times \frac{1}{\sqrt{2\pi} h_c \sigma_c(T)} \cdot \exp\left\{ - \frac{[\log(h_c/\overline{h}_c(T)]^2}{2\sigma_c^2(T)} \right\} \times \frac{1}{\sqrt{2\pi}\sigma_i(T)} \cdot \exp\left(- \frac{h_i^2}{2\sigma_i^2(T)} \right), \qquad (2)$$

with temperature-dependent parameters $\mu_0(T) = \mu_0(1 - T/T_{\rm C})^{\Gamma}$, $\overline{h}_c(t) = \overline{h}_{co}[1 - (T/T_{\rm C})^{\Gamma_c}]$, $\sigma_c(T) = \sigma_{co}[1 - (T/T_{\rm C})^{\Gamma'_c}]$, and $\sigma_i(T) = \sigma_{io}(1 - T/Tc)^{\Gamma_i}$. The temperature dependence of the free energy landscape is thus defined by the four exponents: Γ, Γ_c, Γ'_c and Γ_i. Thermal fluctuations are represented by a thermal viscosity field $h_T^* = (k_B T/\mu_0){\rm Ln}(t_{\rm exp}/\tau_0)$, where $t_{\rm exp}$ is the experimental time constant and τ_0^{-1} is a microscopic attempt frequency. Standard experimental protocols, such as ZFC, FC and various isothermal mag-

netizing sequences, can all be simulated by straightforward Preisach constructions. Reversible processes, such as elastic wall motion and coherent rotation, are treated by assuming that every Barkhausen element contributes an identical reversible term of the form $m_{\rm REV} = \pm[1 - \exp(-\lambda|H_A|)]$ to the total response, so that $m = m_{\rm sat}[(1-f)m_{\rm PREISACH} + fm_{\rm REV}]$, with $0 \leq f \leq 1$.

Numerical simulations of the experimental data based on the generalized Preisach model described above are presented in Fig.1(c). The FC/ZFC simulations in Fig.1(c) have not been superposed on the experimental data in Fig.1(a) for clarity, and to emphasize the systematic structural similarities between the numerical and experimental data. The fitting parameters are listed in Table 1. Considering the simplicity of the mathematical assumptions and the broad spectrum of data, the numerical and experimental response functions are remarkably consistent with each other, as are the two sets of fitting parameters.

Table 1. Preisach fitting parameters by ZFC/FC curves and hysteresis loops.

Parameter	μ_0(emu)	$\overline{h}_{c0}$(Oe)	σ_{c0}	σ_{i0}(Oe)	Γ
ZFC/FC	2×10^{-15}	5200	0.8	104	0.3
loops	2×10^{-15}	5200	0.6	104	0.28-0.32
Parameter	Γ_c	Γ'_c	Γ_i	λ (Oe^{-1})	f
ZFC/FC	5.0	20	0.3	0.208	0.4
loops	4.0	15-20	0.3	0.114-0.182	0.4
Parameter	$m_{\rm sat}$(emu)	$T_{\rm C}(K)$	$\ln(t_{\rm exp}/\tau_0)$		
FC/ZFC	0.8	158	25		
loops	0.8	158	25		

The analysis provides a quantitative picture of the spectrum of Barkhausen moments and free energy barriers of $SrRuO_3$. (1) The collapse of the coercivity as the system is warmed through the ordered phase towards $T_{\rm C}$ is almost exclusively intrinsic in origin and is determined primarily by the exponent Γ_c, with only a negligible contribution from the thermally activated relaxation. Figure 2(b) shows the relationship between the measured coercivity $H_{\rm C}$ and the model coercivity $\overline{h}_c$. (2) The structural characteristics of the ZFC branch are almost purely coercive in origin. The peak in the ZFC moment is a consequence of competition between the collapse of the coercivity distribution as T approaches $T_{\rm C}$ and that of spontaneous moment. The shape of the peak on the low-temperature side is defined by the exponents Γ_c and Γ'_c, and the location of the peak is determined jointly by Γ_c, Γ'_c and μ_0. (3) In contrast, the behaviour of the FC branch is insensitive to the details of the coercivity distribution, and is influenced primarily by the characteristics of the interaction field distribution, i.e. by σ_{io} and Γ_i. The zero-temperature FC moment $m_{\rm FC}(H_A, T=0)$ is determined primarily by the ratio H_A/σ_{io} of the applied field to the dispersion of interaction fields. The weak field dependence of the FC branch observed in $SrRuO_3$ for fields $H_A \geq 500$ Oe is symptomatic of the fact that these fields are much larger than typical interaction fields $\sigma_{i0} = 104$ Oe, and are consequently capable of saturating the FC moment. (4) The pronounced bifurcation of the FC and ZFC branches in low applied fields is a consequence of two inequalities: $\sigma_{i0} << H_A$, which ensures that the FC moment is saturated; and $H_A << \overline{h}_{c0}$, which ensures that the induced ZFC response is small.

3.3. The critical behaviour of $SrRuO_3$

Recently, Kats *et al*[13] obtained the ferromagnetic phase transition and critical behaviour of a $SrRuO_3$ thin film by studying its magnetic resistivity. The critical exponents and Curie temperature of this $SrRuO_3$ thin film were reported as $\gamma = 1.14 \pm 0.07$, $\beta = 0.34 \pm 0.02$ and $T_{\rm C}$=150 K. In this section, we study the quasi-static magnetic response of sintered $SrRuO_3$ in the critical regime and we extract exponent values directly.

Figure 3(a) shows the ac susceptibility measured in various static biasing fields H_A; the application of such fields of increasing strength progressively suppresses the principal (Hopkinson) maximum evident in the zero-field response. The temperatures T_m of these critical maxima shift upwards while their amplitudes decrease as H_A increases. Of particular importance in the present investigation is the result that various critical exponents can be deduced directly from

the maxima evident in Fig.3(a); in contrast, estimates for the exponents γ (from the magnetization above T_C) and β (from the spontaneous magnetization below T_C) frequently involve extrapolation to zero field (to avoid the complications associated with regular contributions to the low field response). The approach advocated here avoids such extrapolations, as the following argument demonstrates. The scaling law equation of state (written in terms of the conventional linear scaling fields $h \sim Hi/T_C$ and $t = |T - T_C|/T_C$) expresses the magnetization (m) and susceptibility (χ) in the vicinity of the ferromagnetic ordering temperature T_C as[14]

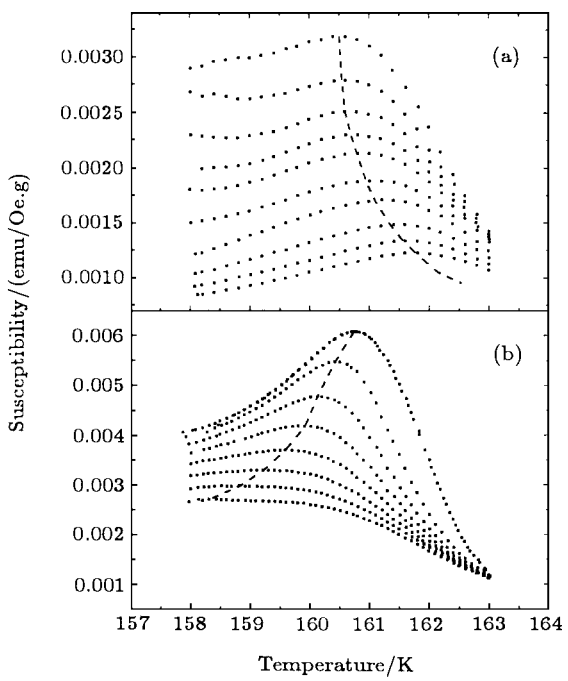


Fig.3. (a) The ac susceptibility as a function of temperature measured in dc biasing fields of 100, 125, 150, 175, 200, 250, 300, 400, 500 and 600 Oe, top to bottom. The dashed line denotes the cross-over line. (b) The ac susceptibility versus temperature at lower dc bias fields, which shows the Hopkinson peaks: from top to bottom, H_A=0, 25, 50, 75, 100, 125, 150, and 175 Oe.

$$\chi(h,t) = \frac{\partial m}{\partial h} = t^{-\gamma} G\left(\frac{h}{t^{\gamma+\beta}}\right), \qquad (3)$$

where G is the derivative (with respect to its argument) of the scaling function F. Assuming the Widom equality $\gamma = \beta(\delta - 1)$ to be valid, this enables the susceptibility to be rewritten as

$$\chi(h,t) = h^{1/\delta - 1} H\left(\frac{h}{t^{\gamma+\beta}}\right), \qquad (4)$$

where $H(X) = X^{\gamma/(\gamma+\beta)} G(X)$. If these (unknown) scaling functions $H(X)$, $G(X)$ or $F(X)$ are universal functions of their argument, then any feature in $H(X)$ will occur at the same value for the variable X. Denoting the reduced temperature of the maxima evident in this figure by $t_m = (T_m - T_C)/T_C$, this analysis leads directly to

$$t_m \propto H_i^{1/(\gamma+\beta)}, \qquad (5)$$

and as the argument X of these scaling functions (H, G or F) is a constant ($X = C$) at such maxima, so are the functions themselves. From Eqs.(3) and (4),

$$\chi(h, t_m) \propto t_m^{-\gamma}, \qquad (6)$$

$$\chi(h, t_m) \propto h^{1/\delta - 1}. \qquad (7)$$

Equations (5), (6) and (7) enable $\gamma + \beta$, γ and δ to be estimated directly from such data, as the following shows. From Eq.(5), plots of the critical peak temperatures T_m against $H_i^{1/(\gamma+\beta)}$ should be linear with the intercept yielding T_C. Such plots have been made for a variety of exponent values, with the best fit obtained with $\gamma+\beta$ values close to those predicted by the mean-field model ($\gamma + \beta = 1.5$), yielding $T_C = 159.7 \pm 0.2$ K. Figure 4(a) confirms both this exponent and T_C estimates; here the reduced peak temperatures, t_m, are plotted against the internal field, H_i, on a double logarithmic scale. The straight line drawn confirms the power-law prediction, Eq.(5), with mean-field model exponents, which yields $\gamma + \beta = 1.50 \pm 0.05$.

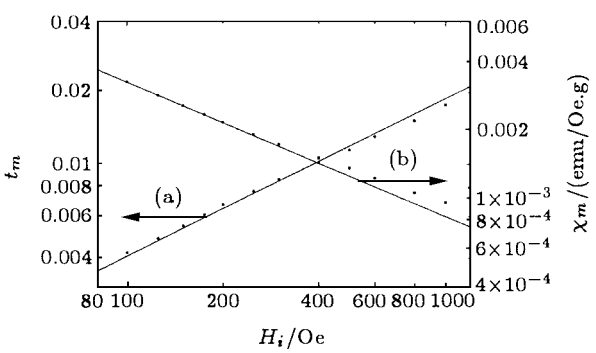


Fig.4. (a) The reduced peak temperature, t_m, versus the internal field, H_i, on a double logarithmic plot. (b) The magnetic susceptibility maxima, χ_m, as a function of the internal field, H_i, measured along the critical isotherm and plotted on a double logarithmic plot.

Having identified T_C, the exponent δ is found directly from the field dependence of the susceptibility measured along the critical isotherm, as shown in Fig.4(b). By using Eq.(7), these data yield $\delta = 2.50 \pm 0.15$, marginally lower than the mean-field model value of 3. But the plot of magnetization versus magnetic field at $T = T_C$ (Fig.5(a)) yields $\delta = 3.17 \pm 0.20$,

which is much closer to the mean-field model value. The exponent γ is found from the data summarized in Fig.3(a) utilizing Eq.(6). Figure 5(b) shows the susceptibility maxima plotted against the reduced peak temperature, t_m, on a double logarithmic scale. These data confirm the power-law prediction, i.e. Eq.(6), and yield $\gamma = 0.96 \pm 0.05$, in agreement with the mean-field model value of 1, within experimental uncertainty.

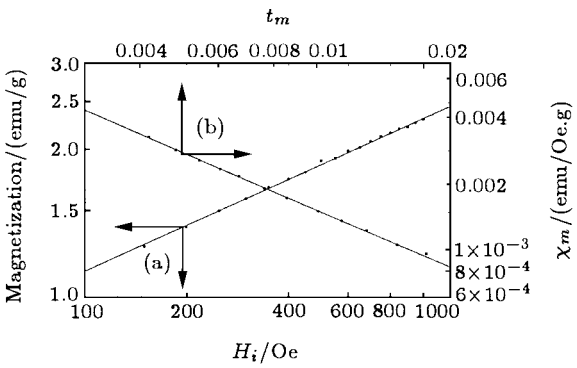


Fig.5. (a) Magnetization as a function of magnetic field at Curie temperature plotted on a double logarithmic plot. (b) The susceptibility maxima χ_m versus the reduced peak temperature, t_m, on a double logarithmic plot.

From data contained in Figs.4 and 5, it is concluded that the sintered $SrRuO_3$ exhibits static magnetic critical exponents consistent with those predicted by the mean-field model. This contrasts with the conclusions reached from recent detailed measurements on perovskite $La_{0.95}Mg_{0.05}MnO_3$,[15] whose critical exponents are in agreement with those predicted by the three-dimensional Heisenberg model. Thus, the possibility is raised that these two types of systems, respectively, may belong to different universality classes. Further theoretical work is necessary to clarify the origin of such differences.

3.4. Is $SrRuO_3$ spin glass?

Reich *et al*[2] recently reported that $SrRuO_3$ shows spin glass behaviour. Some supporting points are as follows. (1) The curve of ac susceptibility versus temperature exhibits a sharp peak with a maximum at 167.6 K, and this maximum shifts to higher temperatures with an increase of the magnetic field. This peak is not a Hopkinson peak, but characteristic of a critical peak. (2) The ac measurements have been performed at three different frequencies, and a shift of the peak with frequency to higher temperature was observed. This trend was considered as characteristic to spin glasses. (3) A large difference between ZFC and FC magnetizations at lower fields was observed, and a cusp in ZFC curve was exhibited; this is again characteristic of spin glasses.

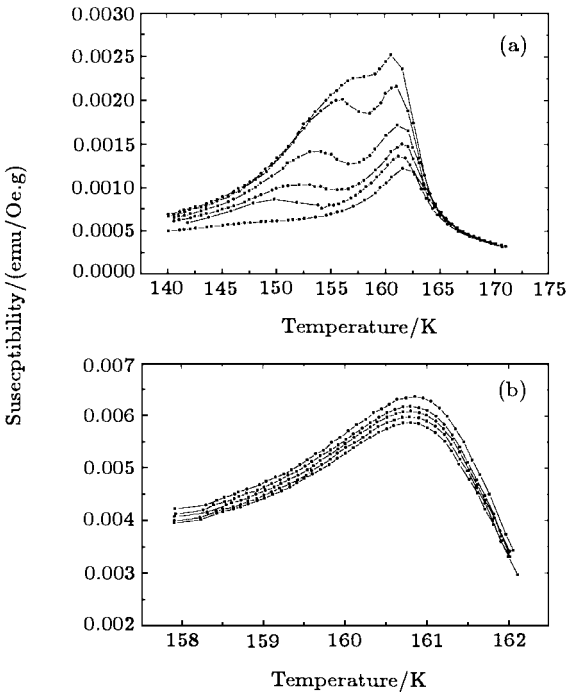


Fig.6. (a) Double peaks of the susceptibility, Hopkinson peak at lower temperature and critical peak at higher temperature: from top to bottom, H_A=150, 200, 300 400, 500 and 600 Oe. (b) The zero-field susceptibility measured at different frequencies: from top to bottom, f=200, 1000, 2000, 4000 and 8000 Hz.

Some measured results below are different from the above points; others are similar to them, but different views are given as the following shows. Figure 3(b) shows the susceptibility versus temperature at lower bias dc fields. These peaks shift to lower temperature as the bias field increases, which is a characteristic of the Hopkinson peak, not that of the critical peak.[14] As the field increases further, the peak splits into two peaks, as shown in Fig.6(a). One peak still shifts to lower temperature, which is the Hopkinson peak. The other shifts to higher temperature, which is the critical peak (also shown in Fig.3(a)). Figure 6(b) shows zero-field susceptibility measured at different frequencies. The peak value decreases with the increase of frequency, but it does not shift to higher temperature as reported in Ref.[2]. The large difference between ZFC and FC magnetizations at lower field (Fig.1(a)) has been discussed in the preceding sections; this is not the behaviour of spin glass. None of the observed results show any characteristics of spin glasses.

4.Conclusion

The ZFC and FC magnetization curves have been measured in a sequence of applied fields. Each ZFC curve peaks at a certain temperature T_P, and the peaks shift to lower temperature as the applied field increases. There is a pronounced bifurcation of the FC and ZFC curves at lower temperatures, while the $M_{\rm ZFC}$ and $M_{\rm FC}$ curves merge together when the temperature is higher than the peak temperature T_P. An empirical model has been proposed to analyse the ZFC behaviours, and the results indicate that the different ZFC behaviours originate from the different temperature dependences of FC magnetization and coercivity.

The ZFC and FC data have also been analysed within the framework of a generalized version of the Preisach model which combines thermal fluctuations with the growth of the free energy barriers. The numerical simulations replicate all of the principal structural systematics of the data, and yield details of the spectrum of Barkhausen instabilities in this material.

The critical temperature and critical exponents have been determined from the ac susceptibility measurements. These exponent values are very close to those predicted by the mean-field model. Our experimental results on $SrRuO_3$ do not show any spin glass behaviours reported previously.

Acknowledgments

We are very grateful to Dr G. Williams, Dr R. M. Roshko, Dr X. Z. Zhou and Dr H. P. Kunkel of the University of Manitoba for their guidance.

References

[1] Kacedon D B, Rao R A and Eom C B 1997 *Appl. Phys. Lett.* **71** 1724
[2] Reich S, Tsabba Y and Cao G 1999 *J. Magn. Magn. Mater.* **202** 119
[3] Kelin L, Dodge J S, Geballe T H and Kapitulnik A 1995 *Appl. Phys. Lett.* **66** 2427
[4] Tan M Q, Tao X M and He J H 2001 *Acta Phys. Sin.* **50** 2203 (in Chinese)
[5] He T and Cava R J 2001 *Phys. Rev.* B **63** 172403
[6] Joy P A, Kumar P S A and Date K A 1998 *J. Phys.: Condens. Matter* **10** 11049
[7] Kumar P S A, Joy P A and Date S K 1998 *J. Phys.: Condens. Matter* **10** L487
[8] Joy P A and Date S K 2000 *J. Magn. Magn. Mater.* **218** 229
[9] Song T, Roshko R M and Dahlberg E D 2001 *J. Phys.: Condens. Matter* **13** 3443
[10] Goya G F, Rechenberg H R and Jiang J Z 2000 *J. Magn. Magn. Mater.* **218** 221
[11] Nam D N H, Jonason K, Nordblad P, Khiem N V and Phuc N X 1999 *Phys. Rev.* B **59** 4189
[12] Bertotti G 1998 *Hysteresis in Magnetism* (New York: Acadamic)
[13] Kats Y, Klein L, Reiner J W, Geballe T H, Beasley M R and Kapitulnik A 2001 *Phys. Rev.* B **63** 054435
[14] Williams G 1991 *Magnetic Susceptibility of Superconductors and Other Spin Systems* ed R. A. Hein *et al* (New York: Plenum) p 475
[15] Zhao J H, Song T, Hunkel H P, Zhou X Z, Roshko R M and Williams G 2001 *J. Phys.: Condens. Matter* **12** 6903